BBA - Bioenergetics 1866 (2025) 149547

Contents lists available at ScienceDirect

BBA - Bioenergetics

journal homepage: www.elsevier.com/locate/bbabio

Engineering of thermal stability in the recombinant xanthorhodopsin from *Salinibacter ruber*

Lada E. Petrovskaya [a,*], Vadim A. Bolshakov [b], Evgeniy P. Lukashev [b], Elena A. Kryukova [a], Eugene G. Maksimov [b], Andrei B. Rubin [b], Dmitriy A. Dolgikh [a,b], Sergei P. Balashov [c], Mikhail P. Kirpichnikov [a,b]

[a] *Shemyakin & Ovchinnikov Institute of Bioorganic Chemistry, Russian Academy of Sciences, ul. Miklukho-Maklaya, 16/10, Moscow 117997, Russia*
[b] *M. V. Lomonosov Moscow State University, Department of Biology, Leninskie gory, 1, Moscow, 119234, Russia*
[c] *Department of Physiology and Biophysics, University of California, Irvine, CA 92697, USA*

ARTICLE INFO

Keywords:
Retinal protein
Xanthorhodopsin
Proton transport
Photocycle
Thermal stability
Hybrid protein

ABSTRACT

Solubilization in detergents is a widely used technique for the isolation of membrane proteins and the study of their properties. Unfortunately, protein stability in detergent micelles can sometimes be compromised. We encountered this issue with xanthorhodopsin (XR) from *Salinibacter ruber*, which had been previously engineered for expression in *Escherichia coli* cells. To explore the factors affecting stability and to enhance thermal stability of recombinant XR preparations following solubilization of membranes using n-dodecyl-β-D-maltopyranoside and nickel-affinity chromatography, we developed a series of hybrid proteins based on the homology between XR and a stable rhodopsin from *Gloeobacter violaceus* (GR). Functional studies of these hybrids and measurements of their melting temperatures revealed the structural elements of XR that account for its notable difference in stability compared to GR, despite their high overall homology of approximately 50 % identical residues.

In particular, XR variants with an engineered loop between transmembrane helices D and E, similar to that in GR, demonstrated enhanced stability. However, we found that replacing the DE loop affects carotenoid binding. Additionally, two hybrid proteins containing the C and D helices from GR exhibited increased stability as well as improved photocycle and proton transport rates. In conclusion, we have demonstrated that optimizing the amino acid sequence of xanthorhodopsin from *S. ruber* based on its homology with *Gloeobacter* rhodopsin is an effective approach to enhance its thermal stability in vitro and improve its potential for optogenetic applications.

1. Introduction

Retinal-containing proteins, which are widely distributed among various microorganisms, utilize the energy of absorbed light to perform important cellular functions [1,2]. Their molecules are composed of seven alpha-helical segments with a covalently attached retinal chromophore in an all-*trans* configuration. Upon light absorption, isomerization of the retinal to the 13-*cis* form initiates a series of conformational changes, leading to alterations in spectral properties and transmembrane charge movements [3,4]. A specific group of microbial rhodopsins from the xanthorhodopsin clade is distinguished by the presence of two chromophores: retinal and carotenoid. The carotenoid functions as a light-harvesting antenna. It absorbs light and part of the excitation energy is transferred to the retinal chromophore thus increasing light-harvesting over a broader spectral range [5]. Xanthorhodopsin (XR) from *Salinibacter ruber* [5,6], the first discovered retinal proton pump with a carotenoid antenna, contains salinixanthin (SX), a 4-ketocarotenoid with a C_{40} chain, a C15 acyl chain and a glycosyl [7]. Analysis of the crystal structure of XR isolated from its native host revealed the interaction interface of XR with SX, which includes several hydrophobic residues from helices E and F. The 4-keto-ring binding pocket contains a small Gly156 residue, which is considered a distinctive feature of carotenoid-binding microbial rhodopsins [8,9]. The configuration of this site facilitates efficient energy transfer from SX to the retinal chromophore, resulting in an expanded light absorption range for XR [10,11].

Abbreviations: BR, bacteriorhodopsin; ESR, retinal protein from *Exiguobacterium sibiricum*; PR, proteorhodopsin; XR, xanthorhodopsin; GR, rhodopsin from Gloeobacter violaceus; DDM, n-dodecyl-β-D-maltopyranoside, SX, salinixanthin; TSA, thermal shift assay.

* Corresponding author at: Shemyakin and Ovchinnikov Institute of Bioorganic Chemistry, ul. Miklukho-Maklaya, 16/10, 117997 Moscow, Russia.
E-mail address: lpetr65@yahoo.com (L.E. Petrovskaya).

https://doi.org/10.1016/j.bbabio.2025.149547
Received 31 October 2024; Received in revised form 9 February 2025; Accepted 10 February 2025
Available online 18 February 2025

Gloeobacter violaceus rhodopsin (GR) is another retinal protein that demonstrated SX binding in vitro, providing efficient (~40 %) energy transfer to retinal [9,12]. It also can bind echinenone [13] and canthaxanthin [14]. GR with bound canthaxanthin exhibited enhanced proton pumping and greater thermal stability compared to the protein without carotenoids [14]. The structure of the carotenoid-binding pocket in GR was investigated by modeling [15] and point mutagenesis, revealing two functional motifs located in helices E and F [16]. Recently, new representatives of XR and PR clades have been shown to bind carotenoids that lack the 4-keto group [17]. This finding has demonstrated that the global distribution of carotenoid-binding rhodopsins encompasses a variety of environments and emphasizes the significance of a detailed investigation of their structure and functions.

Numerous studies focused on deciphering the mechanisms of energy transfer from carotenoids to retinal in XR and homologous rhodopsins, as well as the mechanisms of proton transfer in native cells [5,18], cell membranes and detergents (reviewed in [19]). However, the role of specific amino acid residues in XR was difficult to characterize due to the absence of a suitable expression system. In the recent work [20], we developed a method to produce recombinant XR in *Escherichia coli* cells and demonstrated that its spectral and proton transport properties closely resemble those of the native protein isolated from *S. ruber*. Nonetheless, the purified protein and some of its mutants exhibited limited thermal stability compared to the XR found in native membranes which complicated their characterization [20]. An alternative approach that involved the expression of XR in media with elevated K^+ concentrations yielded functional protein, although some mutants still lacked sufficient stability [21]. Additionally, reduced stability of the recombinant XR produced in a cell-free system was reported in [22]. In the current study, we relied on the homology between XR and thermally stable GR to identify structural elements that affect the thermal stability of recombinant XR. As a result, XR variants with enhanced stability were produced and characterized.

2. Materials and methods

2.1. Plasmid construction

Plasmid pET-XR3 coding for the recombinant XR(1–263) was described earlier [20]. Plasmid pSC-GR containing a wild-type GR gene was a kind gift from Dr. Yu. Bertsova. The genes coding for hybrid proteins were constructed by PCR using primers listed in Table S1. DNA fragments were cloned in pET32a plasmid vector cut with *Nde*I and *Xho*I. Insertions were verified by sequencing (Evrogen). Amino acid sequences of the obtained variants are listed in the Supplementary Material.

2.2. Protein expression and purification

To produce recombinant proteins without carotenoid, *E. coli* C43 (DE3) cells harboring one of the described plasmids were grown at 37 °C in M9 minimal medium supplemented with ampicillin (100 μg/ml) until OD at 600 nm reached ~0.8. Then 0.2 mM IPTG and 5 μM all-*trans*-retinal were added to the medium and incubation continued at 25 °C overnight. Cells were collected by centrifugation at 6000 ×*g* for 20 min. Obtained pellet was resuspended in 50 mM Tris-HCl, pH 8.0, 5 mM EDTA, 20 % sucrose with lysozyme (0.2 mg/ml), and disrupted by sonication. The suspension was centrifuged for 30 min at 6000 ×*g* and the resulting supernatant was centrifuged for 90 min at 100000 ×*g*. Membrane preparation was solubilized in 50 mM Tris-HCl, pH 8.0 containing 1 % n-dodecyl-β-D-maltopyranoside (DDM) and purified on a Ni-affinity column (GE Healthcare) in 30 mM NaP, 200 mM NaCl, 0.05 % DDM, pH 8.0 supplemented with 10–250 mM imidazole. Eluted protein was concentrated and transferred to an imidazole-free buffer using centrifugal filter devices (Ultracel YM-30, Merck Millipore).

To obtain proteins in a carotenoid-bound form, *E. coli* C43(DE3) cells with the pACCAR25ΔcrtXZcrtO plasmid [23] (a gift from Dr. Friedrich) were used. The starting culture (10 ml) was grown in LB with ampicillin (100 μg/ml) and chloramphenicol (34 μg/ml). After reaching OD_{600} ~ 1, the cells were transferred to 400 ml of M9 medium containing the same antibiotics, induced as described above, and cultivated at 25 °C in the presence of all-*trans*-retinal for 48 h after induction. The proteins were purified as described above.

2.3. Spectroscopic measurements

Absorption spectra were recorded on a modified Hitachi-557 (Japan) spectrophotometer. Flash-induced absorption changes of the recombinant proteins were measured with a lab-made flash-photolysis system as described in [24,25]. Before measurements, samples were diluted to A_{540} = 0.1 with complex buffer (5 MM of sodium citrate, MES, MOPS, and CHES, 100 MM NaCl, 0.05 % DDM, pH 7.4). The required pH value was further adjusted by the addition of a small volume of diluted NaOH solution. Flash (532 nm, 8 ns, 10 mJ) was from LS-2131 M Nd-YAG Q-switched laser (LOTIS TII, Belarus). Transient absorption changes were detected by a photomultiplier and digitized by Octopus CompuScope 8327 (GaGe, Canada). The kinetic traces (each was an average of 100 repeats) were fitted with a sum of exponentials using Mathematica (Wolfram Research, USA).

2.4. Proton transport assay

C43(DE3) cells containing one of the described plasmids were grown in 10 ml of M9 supplemented with ampicillin (100 μg/ml) and 5 μM all-*trans*-retinal in 100 ml flasks. After induction with 0.2 mM IPTG at 25 °C overnight, the cells were collected by centrifugation at 3500 x*g* and washed three times with 5 ml of solution containing 10 mM NaCl, 10 mM $MgSO_4$, and 100 μM $CaCl_2$. Between centrifugations, the cells were equilibrated in this solution for 10 min. The cell pellet was resuspended in the same solution (final pH ~5.7) to reach 2 OD at 600 nm in 1 ml. Measurements of light-induced pH changes were performed with a pH electrode (Orion) and Keithley 610C electrometer (USA) equipped with a digital multi-meter Metex 365D (Republic of Korea) as described in [26]. Cell suspension (1 ml) in a thermostated Qpod 2e cell (1 × 1 cm, Quantum Northwest, USA) was illuminated with a 300 W halogen lamp in combination with a 10 cm water IR filter and yellow filter (500–700 nm) at 20 °C with constant stirring.

To normalize the amplitudes of light-induced pH changes in suspensions of cells with expressed proteins, the absorption spectra of the cell suspensions were measured in a 2 mm cuvette positioned at a distance of 4 mm from the photomultiplier of the spectrophotometer. The contribution of Rayleigh scattering was subtracted from the resulting spectra using the inverse fourth power function of the wavelength (see Fig. S1 in the Supplementary Material as an example). The photoinduced pH changes were normalized to the absorbance at the absorption maximum in the 530–550 nm region, which was in the range 0.07–0.12.

2.5. Protein stability measurements

Protein stability was assessed by TSA (thermal shift assay) using a Maya 2000 Pro spectrophotometer (Ocean Optics, USA) with a thermostatically controlled Qpod 2e cell (Quantum Northwest, USA). Protein samples were diluted in 10 mM Tris-HCl, pH 8.0, 100 mM NaCl, 0.05 % DDM to A_{540} = 0.3. The temperature was increased from 30 to 90 °C at a rate of 1°C/min. The spectra were processed using the library tools for the Python SciPy programming language. Rayleigh scattering was subtracted from each spectrum based on the absorption of the sample in the range 700–800 nm. After that, the absorption ratio at the wavelengths of 380 nm (free retinal absorption maximum) and 540 nm (average absorption maximum of the studied retinal proteins) was determined. The change in this ratio accompanying temperature increase was approximated by a sigmoidal function with five parameters Eq. (1) similarly to described in [27]. The melting point was calculated

using the Eq. (2),

$$f(T) = f_{min} + \frac{f_{max} - f_{min}}{\left(1 + e^{\frac{b-T}{a}}\right)^c} \quad (1)$$

$$T_m = b - a^* ln\left(2^{\frac{1}{c}} - 1\right) \quad (2)$$

where a, b, c are the approximation parameters, f_{min} and f_{max} are the minimum and maximum values of the OD380/OD540 ratio correspondingly. A representative fitting example can be found in Supplementary Material (Fig. S2). Results of three independent T_m measurements for each sample were averaged.

3. Results

3.1. Construction and expression of XR-GR hybrid proteins

Replacing protein fragments with amino acid sequences of homologous proteins that possess desired properties is a common approach in protein engineering. This method has also been employed to optimize the amino acid sequences of microbial rhodopsins. To increase the expression level of *Halobacterium salinarum* bacteriorhodopsin (BR) in *E. coli*, its structural elements were replaced with the corresponding fragments from sensory rhodopsin SRII, enabling the production of recombinant BR in sufficient quantities for crystallization [28]. The construction of the hybrid protein C1C2, consisting of five transmembrane segments from the *C. reinhardtii* channelrhodopsin ChR1 and two segments from ChR2, resulted in a high level of expression in the insect cells [29]. Additionally, to enhance the stability of Flavobacteria rhodopsin (FR), several fragments and individual transmembrane helices of this protein were replaced with GPR sequences [30]. Theoretically, the sequential application of this approach allows for the localization of a small region of the target protein that is responsible for its specific properties [28].

To improve the thermal stability of recombinant XR, we propose using this strategy based on the homology of amino acid sequences of XR with the rhodopsin from *G. violaceus* (GR). This protein shares 50 % of its residues with XR (Fig. 1), is efficiently expressed in *E. coli* cells, and exhibits sufficient stability in the absence of a carotenoid [9,14].

In the first step, the genes coding for hybrid proteins Hy1 (which contains the helices A-D from XR and the helices E-G from GR) and Hy2 (includes the helices A-D from GR and the helices E-G from XR) were obtained by PCR. Next, we constructed genes for hybrid proteins with substitutions of smaller structural elements incorporating homologous GR elements in the C-terminal (Hy3–Hy6) and N-terminal (Hy7–Hy10) regions of XR. As a result, we produced 13 gene variants (Fig. 2) which were expressed in *E. coli* C43(DE3) cells with the addition of all-*trans*-retinal.

All strains were cultivated in the M9 minimal medium, which has been previously shown to promote the functional expression of recombinant XR [20]. Electrophoretic analysis of membrane fractions from cell cultures producing hybrid polypeptides revealed the presence of corresponding bands in all samples, except for Hy7 (Fig. S3). The synthesis level was lowest for Hy2, while the highest protein yields were obtained for the Hy8 and Hy9 variants. To study the properties of the hybrid proteins, they were isolated from the membrane fractions after solubilization in DDM and subsequent metal affinity chromatography.

3.2. Hybrids containing helices F and G from GR are unstable

The spectral characteristics of the hybrid proteins are summarized in Table 1. Their absorption maxima varied in the range 533–548 nm. Variants Hy2, Hy3, and Hy8 exhibited blue-shifted absorption maxima, while Hy1, Hy5, and Hy6 demonstrated similar maxima with that of GR (541 nm). Notably, the Hy9 hybrid was the only variant with an absorption maximum close to the recombinant XR (544–548 nm). It should be mentioned that the spectra of several hybrids after purification showed significant light scattering in the short-wavelength region (350–450 nm), and, in some unstable variants, the absorbance of retinal at 360–380 nm (Figs. 3A, B; S4, S5). These features were initially observed in the spectra of the Hy1 and Hy2 hybrids (Fig. 3A, B) and were interpreted as indicators of partial protein denaturation and aggregation due to low thermal stability.

During the construction of the Hy2 variant, we replaced the four XR helices (A-D) with the corresponding structural elements from GR while preserving the sequence of the loop between the helices D and E (DE loop). We also decided to obtain an additional Hy22 variant by replacing the DE loop from XR with the corresponding loop from GR (Fig. 2). The absorption spectrum of the Hy22 demonstrates the decrease in absorption at short wavelengths (Fig. 3C) compared to Hy2, which is consistent with a higher stability of this hybrid (see below).

The hybrid proteins Hy4 and Hy6 exhibited extremely low stability following purification, leading to a rapid loss of retinal that hindered their characterization. Variants Hy3 and Hy5 displayed higher stability; however, their spectra still revealed significant absorption in the short-wavelength region from light scattering and presence of a retinal band (Figs. S4, S5). The hybrid proteins Hy22, Hy8 and Hy9, which demonstrated improved spectral quality, were expected to be more stable (Fig. 3C–E). This assumption was further supported by quantitative measurements using the thermal shift assay (Section 3.4).

3.3. Photocycle characteristics of hybrid proteins

The kinetics of light-induced absorption changes of hybrid proteins in DDM micelles was examined by flash photolysis at four characteristic wavelengths (410, 500, 570, and 620 nm) at pH 9 (Table 2). The initial absorption changes at 620 nm correspond to the formation of a K-like intermediate, and at 570 nm – to the bleaching of the absorption band of the protein in the ground state. The decay of the K intermediate on a microsecond time scale is accompanied by a decrease in absorption at 620 nm. It is followed by an increase in absorption at 410 nm which reflects accumulation of the M intermediate from deprotonation of the Schiff base and proton transfer to the proton acceptor (Asp96 in XR). The subsequent decrease in absorption at 410 nm and simultaneous increase at 570 nm reflect the decay of the M-state and formation of the N intermediate during reprotonation of the Schiff base. The next transition (N → O) is characterized by an increase in absorption with a maximum at 620 nm. The decay of the O state and the return of the initial state led to a decrease in absorption at 620 nm and a simultaneous increase at 570 nm.

The overall duration of the photocycle and the parameters of its kinetic stages varied significantly among the hybrid proteins (Table 2, Fig. 4). The Hy1 variant exhibits a fast photocycle, characterized by the absence of detectable accumulation of the M intermediate. Long-wave products dominate the photocycle of this protein (Fig. 4C). As previously demonstrated for PR [33] and ESR [34], the absence of visible M formation may be attributed to kinetic reasons (the rate of its decay exceeds the rate of formation). In this case, an increase in pH and a corresponding slowdown in the Schiff base deprotonation rate should enable the detection of M formation. However, attempts to study this hybrid at higher pH values were unsuccessful due to its instability under these conditions.

The photocycle of the Hy2 hybrid, on the contrary, is characterized by a substantial amount of the intermediate M (Fig. 4D), which is formed with $\tau_1 \sim 5$ μs and $\tau_2 \sim 48$ μs at pH 9 (Table 2). The decay of M occurs in several stages and ends with a return to the initial state with $\tau \sim 700$ ms. The formation of red-shifted intermediates at 620 nm is not observed, suggesting a delay in the Schiff base reprotonation. Overall, the photocycle of this variant is significantly slower compared to the Hy1 and XR proteins. In the Hy22 hybrid, the formation of M occurs more rapidly with two time constants of 1.7 and 9 μs. Additionally, the decay of M and

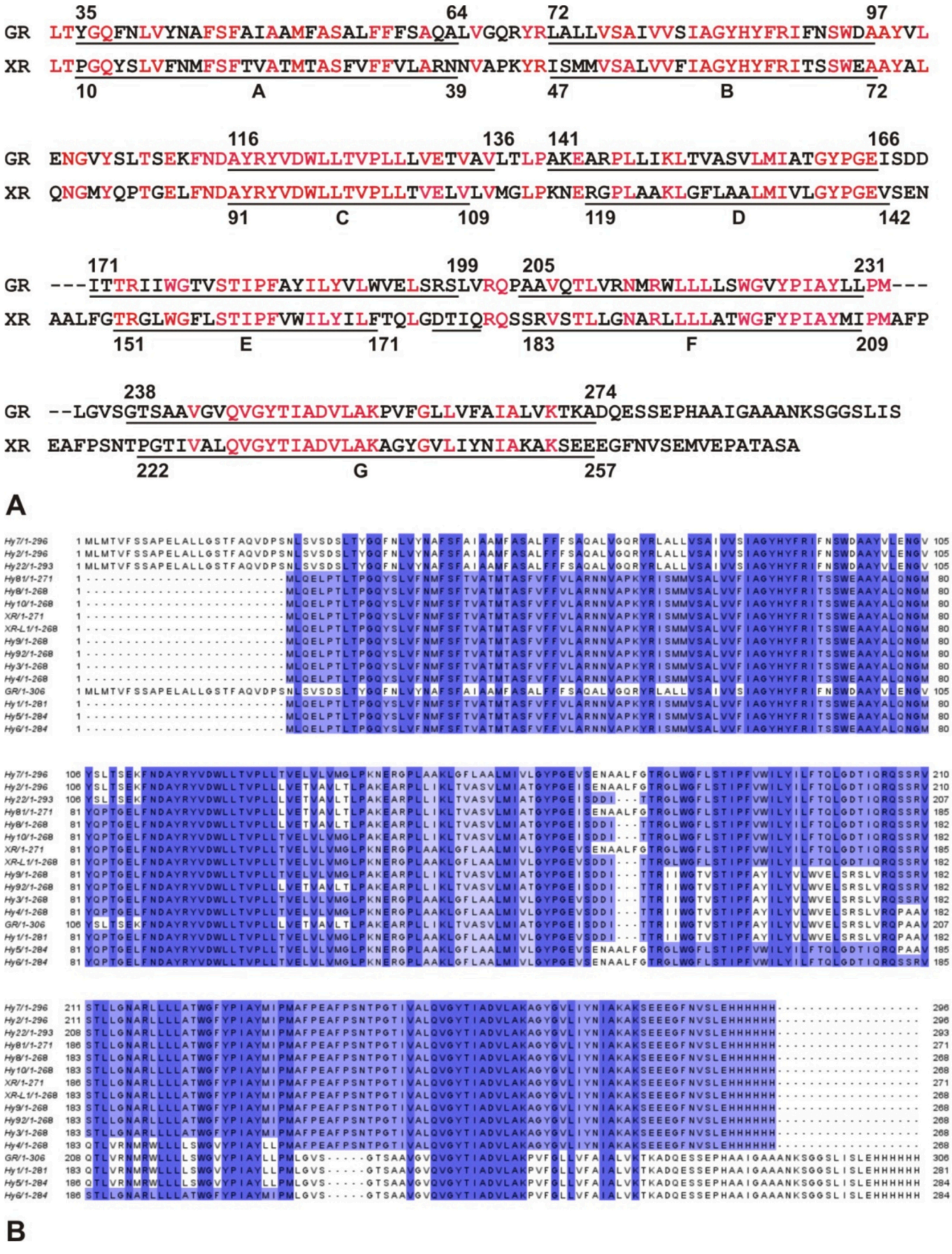

Fig. 1. A) Partial amino acid sequence alignment of GR and XR using BLAST. The positions of the helical segments A-G according to PDB ID 6NWD and 3DDL, correspondingly, are indicated. Identical residues are shown in red letters. B) Multiple sequence alignment of XR, GR and hybrid proteins using Clustal Omega. Color was applied according to percentage identity. (For interpretation of the references to color in this figure legend, the reader is referred to the web version of this article.)

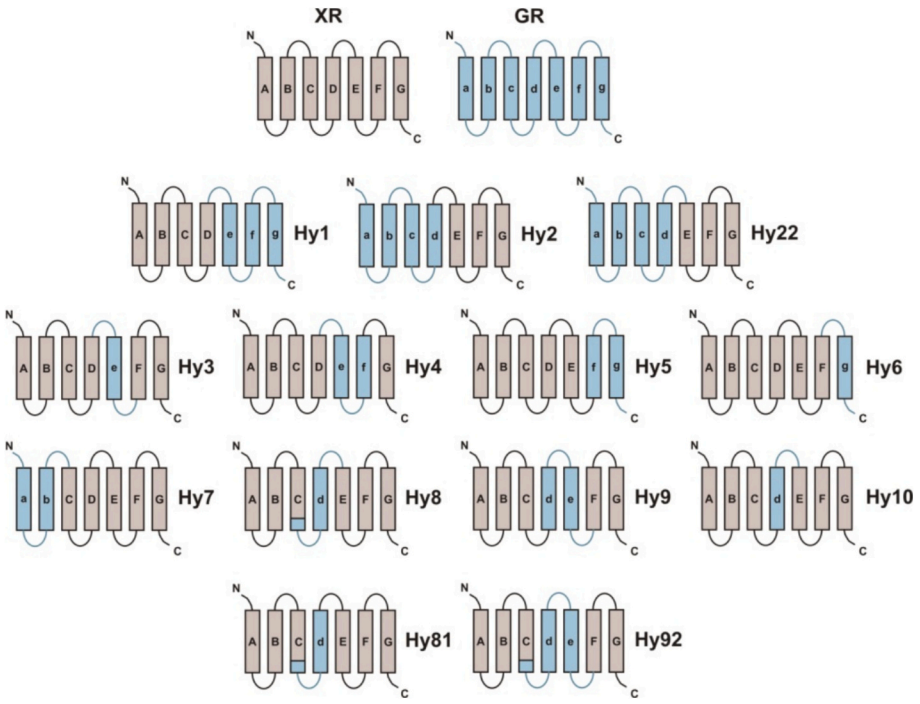

Fig. 2. Structural schemes of hybrid proteins. Structural elements derived from XR are shown in grey, and those from GR are in light blue. (For interpretation of the references to color in this figure legend, the reader is referred to the web version of this article.)

Table 1
Spectral characteristics of hybrid proteins.

Protein	Structure (helices)	λ_{max}, nm at pH 9	Spectral quality
GR [31]	abcdefg	541	High
XR from *S. ruber* [32]	ABCDEFG	551–553	High
XR from *E. coli* [20]	ABCDEFG	544–548	Low[a]
Hy1	ABCDefg	538	Low
Hy2	abcdEFG	533	Low
Hy22	abcdEFG	533	High
Hy3	ABCDeFG	535	Low
Hy4	ABCDefG	nd	Low
Hy5	ABCDEfg	541	Low
Hy6	ABCDEFg	541–544	Low
Hy8	ABcdEFG	534–536	High
Hy9	ABCdeFG	544–548	High
Hy92	ABCdeFG	544–548	High
Hy10	ABCdEFG	537	Low
XR-L1	ABCDEFG	544–548	High

[a] Significant absorption in the short wavelength region (350–450 nm), mainly due to light scattering and, in some variants, to the retinal absorption band, was interpreted as low spectral quality.

the return to the initial state in Hy2.2 are significantly accelerated compared to Hy2.

The Hy8 hybrid protein exhibits one of the fastest photocycle rates among all the studied variants (Table 2). It is considerably faster than that of the recombinant XR. At pH 9, the formation of M is characterized by kinetics including three components with 2, 18, and 69 μs time constants, while the decay of M occurs with τ ~5.3 ms. The return to the initial state takes place with τ ~26 and 126 ms (Fig. 4E).

In the photocycle of Hy9, the formation of the intermediate M occurs with characteristic time constants of 7 and 40 μs at pH 9, and its decay occurs with time constants of 2.5 and 9 ms. The decay of long-wave intermediates and the return to the initial state are described by characteristic time constants of 99 and 356 ms, respectively (Fig. 4F). Thus, the reprotonation of the Schiff base in Hy9 is relatively slowed compared to the recombinant XR.

3.4. The presence of the DE loop from GR increases thermal stability in XR mutants

Thermal stability is an important characteristic of recombinant proteins since it enables the assessment of functional and structural changes in mutant variants compared to native proteins. In this study, we investigated thermal stability of hybrid proteins by measuring their melting curves upon heating from 30 to 90 °C (Fig. S6) and calculating the phase transition temperature (T_m) at which 50 % of the protein is denatured (thermal shift assay, TSA). Previous studies have shown that the denaturation of retinal proteins is accompanied by the Schiff base hydrolysis and accumulation of unbound retinal in protein samples [35]. Additionally, light scattering from protein misfolding and aggregation contributes to the absorption spectra in the short-wavelength region

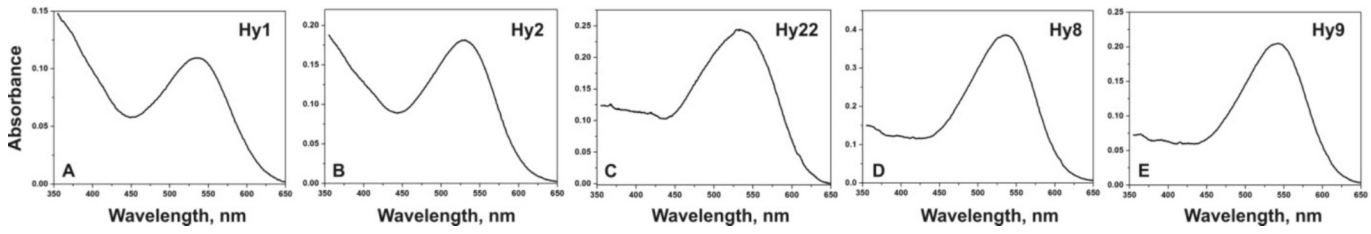

Fig. 3. Absorption spectra of selected hybrid proteins in the complex buffer at pH 9.0.

Table 2
Photocycle characteristics of hybrid proteins.

Protein	τ_1, μs	τ_2, μs	τ_3, ms	τ_4, ms	τ_5, ms	τ_6, ms
GR [31]	11	110	0.640	3.2	22	140
GR (this study)	6.7	131	0.467	4.1	44	209
XR from *S. ruber* [5][a]	7.5	35	0.280	1.3	11	100
XR from *S. ruber* [32][b]	8.2	45	0.144	0.5	5	343
XR from *E. coli* [20][c]	3.4	45	0.175	1.6	63	226
Hy1	3.8	33	0.510	1.8	55	228
Hy2	5.2	48	–	4.3	76	698
Hy22	1.7	9	1.83	14.6	55	272
Hy3	7.6	53	0.615	3.9	28	530
Hy5	3	53	–	1.2	83	253
Hy8	2	18	0.069	5.3	26	126
Hy9	7	40	2.5	9.2	99	356
Hy92	9.4	35	0.32	3.5	11	31
Hy10	3,3	27	0.91	9.3	219	1129
XR-L1[c]	4.9	58	0.41	4.0	21	350

In the photocycle of the recombinant XR, τ_1 and τ_2 constants correspond to M intermediate formation, τ_3 and τ_4 reflect the decay of the M-state and formation of the N/O intermediate, τ_5 and τ_6, the decay of the O state and return of the initial state. Assignment of the rate constants for individual proteins can vary, see corresponding text.

[a] Membranes of *S. ruber* solubilized with 0.15 % DDM at pH 8.8.
[b] Membranes of *S. ruber* after bleaching of SX at pH 8.6.
[c] At pH 8.0. Other time constants were obtained at pH 9.0.

(350–450 nm). Therefore, we selected the ratio of absorption at 380 nm to that at 540 nm (the average absorption maximum of the studied proteins) as a criterion for assessing protein state in our studies.

We have previously demonstrated that the recombinant XR in the absence of a carotenoid exhibits low stability and quickly loses its color [20]. Therefore, we were unable to measure its melting point using TSA. In contrast, the carotenoid-bound form of the same protein (see below) displayed higher stability, which enabled us to determine the corresponding value (64 °C). For comparison, we also obtained data for the recombinant GR. Its melting temperature was ~74 °C, and in the complex with carotenoid, it increased to 81 °C (Table 3).

The study of hybrid proteins using TSA revealed their different thermal stability. The Hy1 and Hy2 variants, which exhibited low spectral quality, demonstrated relatively low melting temperatures (58 and 61 °C, respectively). As a result of replacing the DE loop from XR with the corresponding GR loop in the Hy22 variant, we observed an increase in the melting temperature by 10 °C, up to ~71 °C. The most significant increase in stability was demonstrated by the Hy8 and Hy9 variants (T_m 77 and 76 °C, respectively). Consequently, the stability of these variants exceeded that of the carotenoid-free recombinant GR. An even higher T_m (79 °C) was exhibited by the Hy92 variant of the Hy9 hybrid, in which the CD loop was exchanged with that from GR (see below).

To confirm the role of the DE loop in the thermal stabilization of hybrid proteins, we constructed the XR variant containing the corresponding sequence, XR-L1. The absorption maximum of this protein was 544–548 nm at pH 8, which corresponds to the previously determined

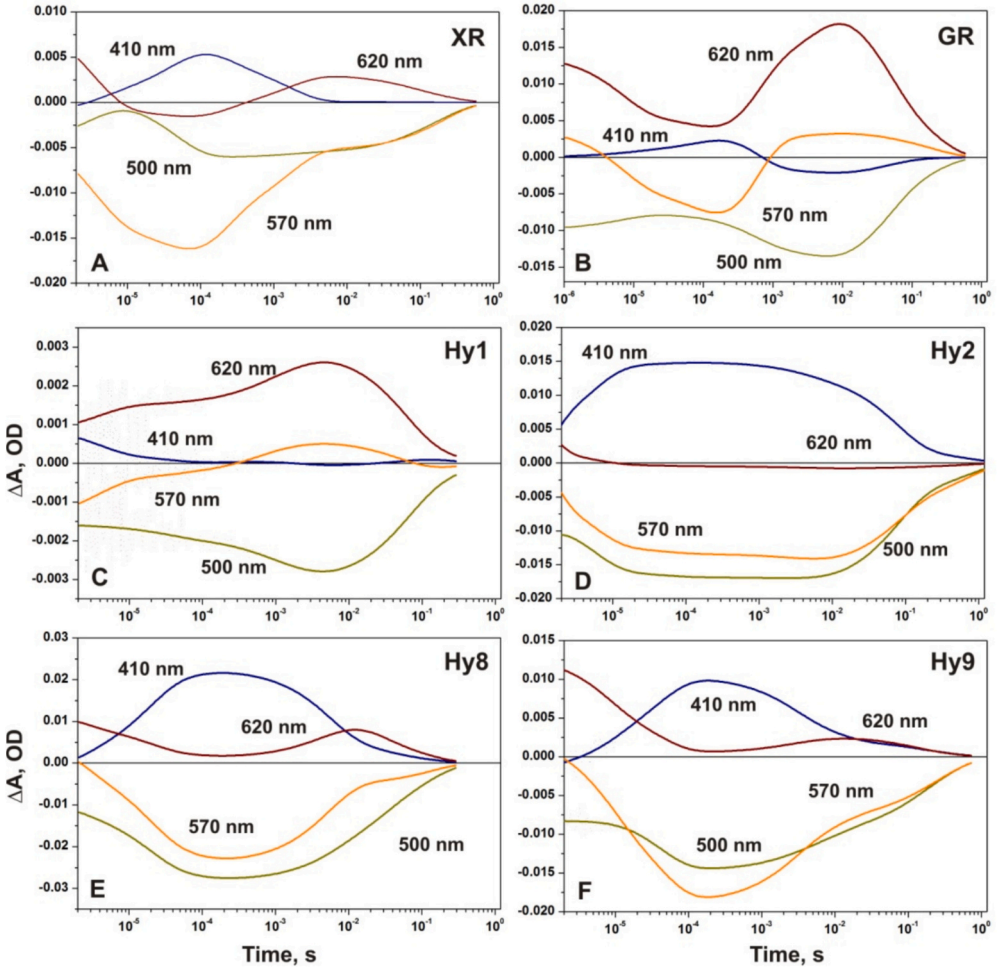

Fig. 4. Light-induced absorption changes at 410, 500, 570, and 620 nm of the recombinant XR (A), GR (B), Hy1 (C), Hy2 (D), Hy8 (E), and Hy9 (F) hybrid proteins. Samples were in the complex buffer (pH 9.0) containing 0.05 % DDM and 100 mM NaCl. Data for XR are from [20].

Table 3
The melting temperatures of hybrid proteins. The mean and STD from three independent experiments are shown.

Protein	T_m, °C
GR	73.5 ± 0.4
GRC[a]	80.7 ± 0.3
XRC[a]	64.6 ± 0.5
Hy1	58.5 ± 0.6
Hy2	60.8 ± 0.2
Hy22	70.7 ± 0.4
Hy3	66.1 ± 0.3
Hy8	77.4 ± 0.5
Hy9	75.5 ± 0.6
Hy92	79.0 ± 0.4
XR-L1	67.5 ± 0.2

[a] GRC, XRC – carotenoid-bound forms of GR and XR, correspondingly.

value for the recombinant XR [20] (Fig. 5A). Notably, the absorption at shorter wavelengths in the spectrum of XR-L1 is significantly lower compared to that of the recombinant XR, indicating its higher stability. The photocycle of XR-L1 (Fig. 5B) includes the main intermediates, the formation and decay of which can be described by a set of six time constants. At pH 8, the formation of the M intermediate occurs with time constants of 5 and 58 ms, and its decay with τ ~0.4 and 4 ms is accompanied by the formation of long-wavelength intermediates of the photocycle. Their decay and return to the initial state are described by τ ~21 and 350 ms (Table 2). Thus, reprotonation of the Schiff base in this protein is somewhat slowed compared to the recombinant XR; however, the kinetic constant for this step is similar to that of XR isolated from *S. ruber* and bleached from SX [32]. The melting temperature of XR-L1 is 67.5 °C, which exceeds the value for the recombinant XR in the carotenoid-bound form.

3.5. Modification of the amino acid sequence between C and D helices increases the photocycle rate in XR hybrid variants

Comparison of the amino acid sequences of the helix C in XR and GR reveals their strong conservation up to the cytoplasmic region. The sequence of this region and the CD loop is less conserved (Fig. 1). To understand the structural basis for the fast photocycle observed in the Hy8 hybrid variant (which includes the cytoplasmic part of the helix C and the helix D from GR), we modified the amino acid sequence of the Hy9 hybrid (which contains the helices D and E from GR) by replacing the sequence of the cytoplasmic part of the helix C and the loop between the helices C and D (CD loop) with those from GR. The resulting protein Hy92 exhibited good spectral properties (Fig. 6A) and a fast photocycle (Table 2, Fig. 6B). The rate of the M intermediate formation in this protein is characterized by three time constants of 9, 35 and 320 μs. The first two constants are comparable to those of Hy9 while the third one is about eight times smaller. Also, the τ_4 time constant (3.5 ms), which describes the M decay in Hy92, is ~2.5 times smaller than in Hy9. Return to the ground state in Hy92 occurs with time constants 11 and 31 ms indicating a substantial acceleration of this process when compared to Hy9 (9 and 11.5-fold decrease of τ_5 and τ_6 correspondingly).

The Hy92 also demonstrated acceleration of the final photocycle stages compared to Hy8. The τ_5 and τ_6 time constants of its photocycle were respectively 2.5 and 4 times smaller (Table 2). As a result, Hy92 exhibited the highest photocycle rate observed in our study. Additionally, its thermal stability exceeds those of the Hy8 and Hy9 hybrids (melting temperature is 1.5 and 3.5° higher than those of Hy8 and Hy9, respectively).

3.6. Proton transport in E. coli cells with expressed hybrid proteins

To evaluate the ability of hybrid proteins to transport protons across the membrane, we measured light-induced pH changes in suspensions of *E. coli* cells expressing the variants Hy8, Hy9, Hy92, and XR-L1. The same cells producing GR and XR were used as controls. For all samples studied, illumination of the suspension resulted in the acidification of the medium similar to that observed in the cells with XR and GR expression. However, the speed and amplitude of this process vary considerably among the different hybrid proteins (Fig. S7, Fig. 7).

The cell suspensions containing Hy9 and XR-L1 exhibited amplitudes of pH changes that were 1.5 and three times smaller, respectively, than those observed with XR, despite comparable levels of recombinant proteins expression (Figs. 7A, S1). In contrast, the normalized amplitudes of the light-induced pH changes in the suspensions of *E. coli* cells producing the Hy8 and Hy92 variants were almost 1.5 times greater. Additionally, they were two times higher than that of the pH changes observed in *E. coli* cells expressing GR (Fig. 7B). Thus, in our study, the Hy8 and Hy92 hybrids emerged as the most efficient variants in terms of photocycle rate and proton transport.

3.7. Increased stability correlates with impaired ability to bind carotenoids in XR variants containing DE loop from GR

In the previous work, we demonstrated that the recombinant XR can bind salinixanthin (SX), a major carotenoid found in *S. ruber* cells [20]. The reconstitution of the recombinant GR with SX [9] and echinenone

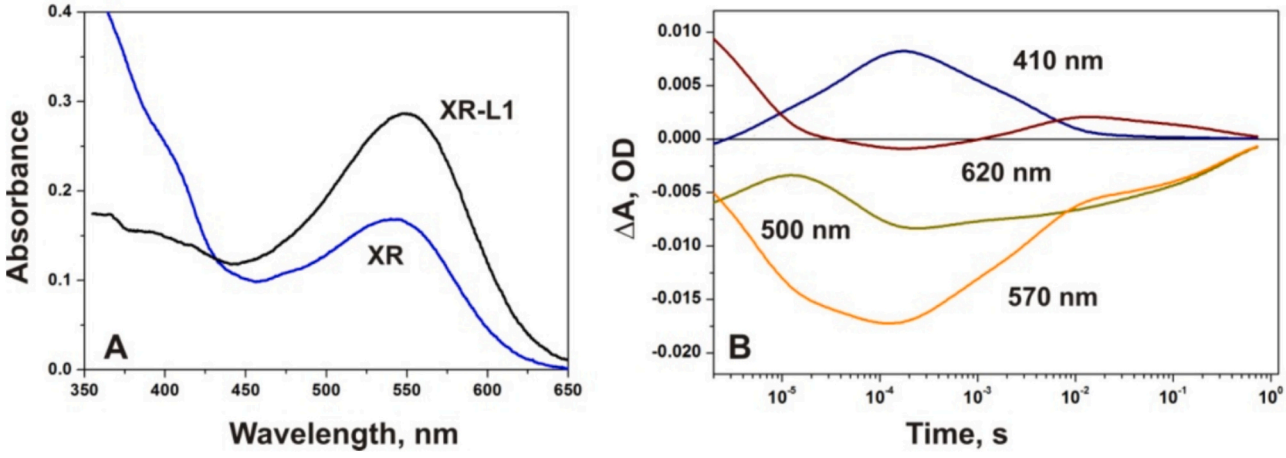

Fig. 5. Properties of the XR-L1 mutant. A) Absorption spectra of the XR-L1 and the recombinant XR [20] at pH 8.0. B) Kinetics of light-induced absorption changes of the XR-L1 at 410, 500, 570, and 620 nm (pH 8.0).

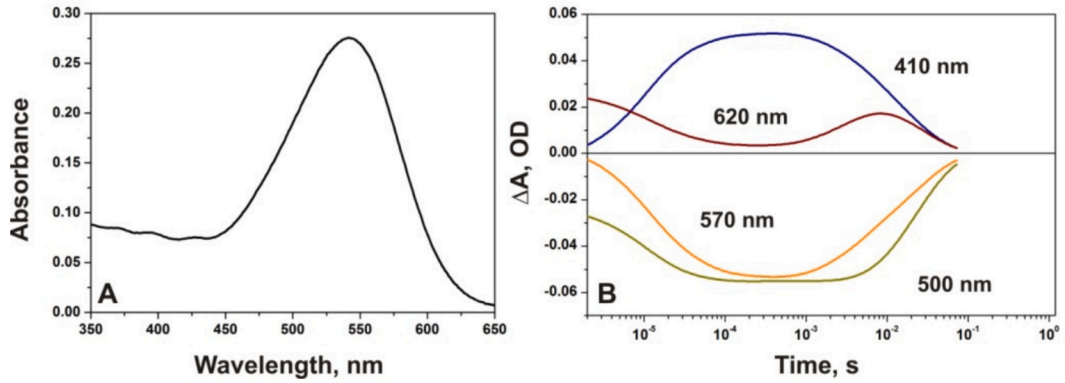

Fig. 6. Properties of the Hy92 hybrid. A) Absorption spectrum. B) Kinetics of light-induced absorption changes at 410, 500, 570, and 620 nm at pH 9.0.

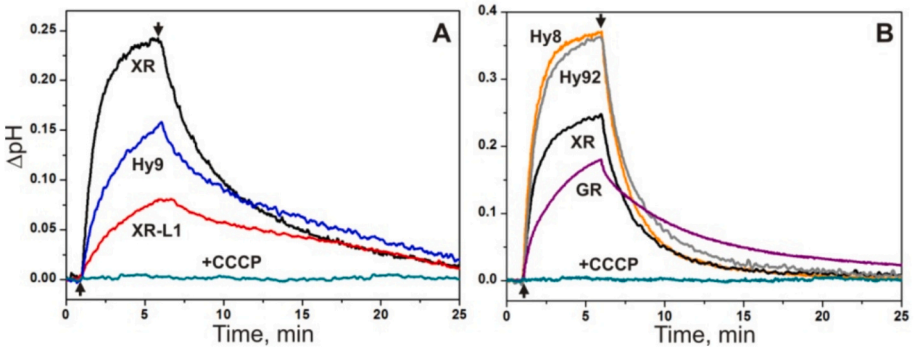

Fig. 7. Light-induced pH decrease in *E. coli* cell suspensions containing: A) recombinant XR (black line), Hy9 (blue line), and XR-L1 (red line). B) Hy8 (orange line), Hy92 (grey line), recombinant XR (black line), and GR (purple line). Green line – pH changes in the suspension of cells containing recombinant XR (A) or Hy8 (B) in the presence of 10 μM carbonyl cyanide *m*-chlorophenyl hydrazone (CCCP). The arrows indicate the light turning on and off. The amplitudes of light-induced pH changes were normalized for retinal protein content in the samples. (For interpretation of the references to color in this figure legend, the reader is referred to the web version of this article.)

[13] was previously reported. GR can be also expressed in *E. coli* in the presence of endogenously produced keto-carotenoids [14]. In the current study, to characterize the ability of the hybrid proteins to bind carotenoids, we isolated recombinant proteins from *E. coli* cells harboring the pACCAR25ΔcrtXZcrtO plasmid. The *crtO* gene encodes β-carotene ketolase which converts β-carotene into echinenone and canthaxanthin [36]. The presence of both keto-carotenoids in these cells has been demonstrated previously [37]. Since GR can bind to either of them [13,14], we suppose that the recombinant proteins derived from the carotenoid-producing strain may contain a mixture of echinenone- and canthaxanthin-associated forms.

For the control, the recombinant XR was obtained from the same strain. The absorption spectrum of the purified protein displayed additional maxima at ~430, 458, and 485 nm indicating the presence of carotenoids. Notably, the absorption value at 485 nm was twice as high as that at 546 nm (Fig. 8A) suggesting effective carotenoid binding. It should be mentioned that the vibronic structure characteristic of the spectrum of SX-bound XR [5,20] was not observed in this sample.

When the hybrid proteins Hy8, Hy9, and XR-L1 were produced under the same conditions, the corresponding bands were only seen in the absorption spectrum of the Hy9 variant (Fig. 8B). It is noteworthy that the absorption value at these wavelengths did not exceed the absorption in the band associated with the bound retinal. We presume that in Hy9 only a small fraction of the protein is in a carotenoid-bound state. In contrast, the absorption spectra of the Hy8 and XR-L1 variants grown under the same conditions did not show any additional maxima

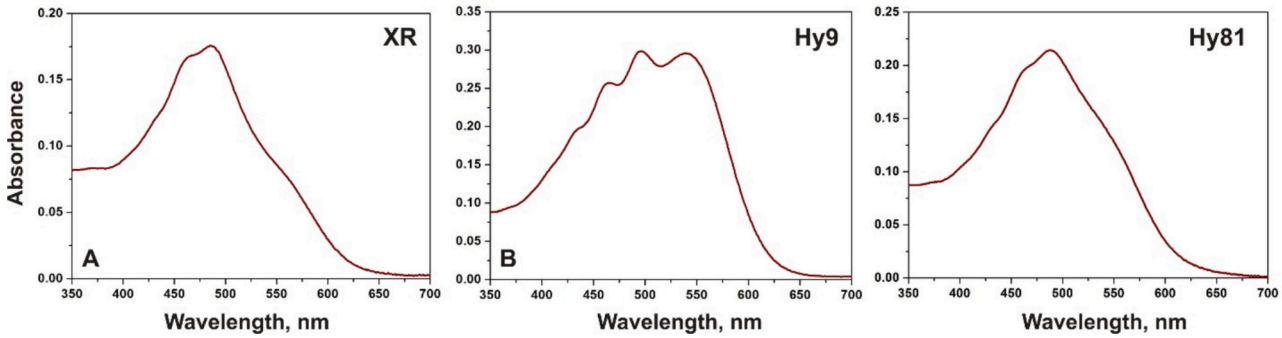

Fig. 8. Absorption spectra of the recombinant XR (A), the Hy9 variant (B) and the Hy81 variant (C) obtained from the carotenoid-producing *E. coli* cells. Samples were in the complex buffer, pH 8.0.

indicating the presence of a bound carotenoid. Consequently, their spectra resembled those of the same proteins obtained from the strain without carotenoid production (Fig. S8A, B). Notably, the cells co-expressing these variants and carotenoids demonstrated a characteristic red color that was different from the color of the cells without carotenoid production (Fig. S8C).

To confirm the role of the DE loop in carotenoid binding by XR, we replaced this sequence in the Hy8 variant with the corresponding loop from XR. The spectrum of the Hy81 hybrid obtained from the carotenoid-producing strain demonstrated the presence of characteristic bands (Fig. 8C), indicating a carotenoid-bound state similar to that of the recombinant XR. However, judging by the lower ratio of absorption at 485 nm to that at the retinal absorption maximum (1.42 vs ~2 in XR), the carotenoid content in Hy81 was lower than in XR (Fig. 8A).

4. Discussion

Solubilization in detergent micelles is the most commonly used approach to isolate target membrane proteins from surrounding lipids and other proteins, allowing for the study of their structure and properties. Several mild detergents are available that do not affect the functional state of the proteins [38,39]. However, the stability of certain proteins in micelles may be compromised, presumably due to the absence of specific lipids and/or loss of structural integrity. Several examples of retinal proteins that rapidly lose their native conformation in solubilized form are known. In [40] the photobleaching of monomeric BR in octyl glucoside micelles was reported. Sensory rhodopsin I from *H. salinarum* [41] and a retinal protein FR from Flavobacteria [30] demonstrated extremely low stability after purification in detergent. We previously encountered a similar problem with recombinant XR produced in *E. coli* cells and purified in DDM micelles [20], unlike XR obtained by solubilization of native cell membrane fragments from *S. ruber* which remained stable [42].

Site-directed mutagenesis, including mutations of single residues [43] or changes of the secondary structure elements [30] has been successfully utilized to enhance the thermal stability of retinal proteins. To explore factors affecting the stability of recombinant XR and to improve the properties of its mutant variants, we constructed hybrid proteins containing fragments from its close homolog, *Gloeobacter* rhodopsin (GR). We were inspired by the remarkable difference in thermal stability between recombinant XR and GR despite the high degree of sequence homology between the two proteins. Using this approach, we aimed to identify regions of the XR amino acid sequence associated with its reduced stability which could potentially be optimized in order to improve it.

Structural studies of GR have revealed several features that may contribute to its greater thermal stability. The GR molecule is characterized by denser packing on the extracellular side of the protein compared to XR which leads to a displacement of the transmembrane helices E and G towards the center of the alpha-helical bundle [15]. In particular, the interaction between Tyr249 and Glu166, along with the salt bridge between Glu166 and Arg174 may contribute to such properties. As a result, the retinal binding pocket of GR apparently has a larger size than that of XR due to the inclusion of two tyrosine residues, Tyr119 and Tyr249. In XR, the homologous Tyr94 and Tyr232 are positioned at a greater distance from the retinal (Fig. 9). It is important to note that the GR structure was obtained in the absence of a carotenoid. It demonstrates tighter packing compared to the XR structure, which includes SX [15]. To confirm this hypothesis, it would be necessary to compare the structures of carotenoid-free and carotenoid-bound forms of one rhodopsin, which are not currently available.

In the current study, we have demonstrated that several hybrid proteins containing the DE loop sequence from GR exhibit increased stability. Notably, the length of this loop is shorter in the GR molecule (4 amino acid residues compared to 8 residues in XR, Fig. 1) and, as a result, the distance between Glu166 and Arg174 in GR is 2.89 Å,

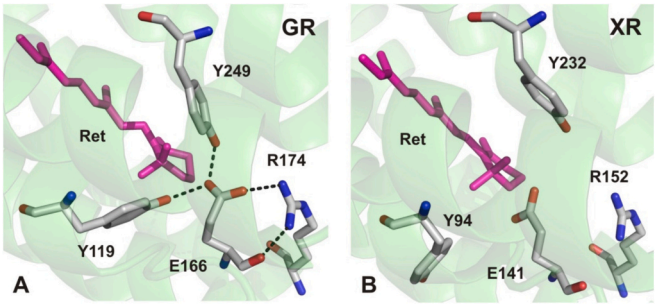

Fig. 9. Structural comparison of GR and XR. Selected amino acid residues from D, E and G helices and all-*trans* retinal (Ret) are shown based on PDB entries 6WND and 3DDL, respectively. Polar contacts inside the selection identified with PyMol are depicted as black dots.

whereas in the XR molecule, the homologous Glu141 and Arg152 are separated by 4.8 Å. This distance exceeds 4 Å, which allows the formation of a salt bridge. The direct evidence for the effect of the DE loop displacement is the observed 10 °C increase in the melting point of the Hy22 hybrid compared to the Hy2 variant.

To further confirm the role of the DE loop in increasing the stability of XR mutants, we introduced an appropriate substitution in the XR amino acid sequence, resulting in the XR-L1 mutant. Since the melting point of the XR in carotenoid-free form could not be determined due to its low stability, only an indirect comparison of these proteins was feasible. Firstly, the spectrum of the XR-L1 is characterized by the absence of significant light scattering and an increase in absorption at 380 nm, indicating the release of retinal as a result of the hydrolysis of the Schiff base. Secondly, it has been shown for several retinal proteins that the formation of a complex with a carotenoid enhances their thermal stability [14,44]. The measured melting point of the carotenoid-bound form of XR was 64 °C. For GR, the increase in melting point of the carotenoid-bound protein compared to the carotenoid-free form was approximately 7 °C (Table 2). Assuming a similar shift for XR, the melting point of its carotenoid-free form could be estimated to be around 57 °C. Consequently, the addition of the DE loop from GR contributed to a 10 °C increase in the melting point of XR (to 67 °C), similar to the effect observed in the Hy2 hybrid. Of course, this estimate is approximate and should be validated by further studies.

It should be mentioned that the Hy10 variant, which includes the DE loop and the helix D from GR, did not show any significant changes in stability compared to XR. In contrast, the hybrid proteins Hy8 and Hy9, which contain the DE loop sequence from GR, demonstrated significantly higher stability (an increase in melting temperature of 10 and 8 °C, respectively, compared to XR-L1). In addition to the increased thermal stability, the Hy8 variant is characterized by an accelerated photocycle and high efficiency of proton transport in *E. coli* cells. Given the highly conservative sequence of the helix C, the difference between the stable Hy8 variant and the unstable Hy10 is in the sequence of the cytoplasmic end of this helix and the CD loop (Fig. 1). We assume that these elements of the GR sequence also contribute to its increased stability compared to XR.

The Hy9 hybrid protein demonstrated only a slight decrease in stability compared to the Hy8 (T_m lower by 2 °C), however, the characteristic time constants of its photocycle were significantly larger (Table 2) and the efficiency of proton transport was lower (Fig. 7A). In order to assess the effect of the sequence differences between these two proteins on their photocycle rates, we constructed and characterized a modified Hy92 variant which contains, in addition to the helices D and E, the cytoplasmic part of the helix C and the loop between helices C and D from GR. The resulting protein demonstrated increased stability and a faster photocycle rate, even compared to Hy8.

In most cases, the photocycle kinetics of microbial proton pumps is determined by the rate of the Schiff base reprotonation during the M →

N transition and the subsequent return to the ground state (decay of N and O intermediates). To ensure fast reprotonation of the Schiff base in retinal proteins, 1) an efficient donor residue with an appropriate pK_a should be present and 2) it should be positioned in an appropriate configuration (distance and environment) relative to the Schiff base. All the hybrid proteins studied contain a glutamate residue in the cytoplasmic part of the helix C, which acts as a proton donor in XR and GR (Glu107/132). However, even in some of the relatively stable variants (i.e. Hy22 and Hy9), the final stages of the photocycle are decelerated (time constants τ_4-τ_6 are increased compared to XR, Table 2). In contrast, the Hy8 and Hy92 variants which contain the corresponding region of the helix C and the CD loop from GR demonstrated significantly increased photocycle rates.

Helix C in bacteriorhodopsin-related proton pumps contains both proton acceptor (Asp85 in BR) and donor (Asp96 in BR) residues and plays a crucial role in proton transfer reactions [45,46]. Reprotonation of the Schiff base is considered to occur as a result of proton transfer through the chain of interacting residues and bound water molecules in the cytoplasmic part of a protein rather than a simple act of proton migration from the donor [47]. Therefore, the overall structure of this protein region determines the resulting efficiency of the reprotonation process. The importance of the loop sequences for the folding, stability and functional activity of the retinal proton pumps has previously been reported for BR [48–50] and PR [51,52]. Specifically, conformational changes in the CD loop during the M → N transition have been observed in BR [53]. We can conclude that the configuration of the C—D region in GR is advantageous for the rapid transfer of protons to the Schiff base compared to XR. The introduction of the corresponding sequence into XR positively affects the rate of the M state decay and return to the ground state in hybrid variants. Undoubtedly, further studies are needed to elucidate the structural basis for the observed effects

The presence of an additional carotenoid antenna expands the range of absorbed light energy, ultimately increasing the efficiency of light energy captured by retinal proteins. It is therefore desirable to retain the ability to bind carotenoids in optimized hybrid proteins. We assessed the ability of the proteins Hy8, Hy9, and XR-L1 to bind carotenoids by co-expression in *E. coli* cells producing the corresponding enzymes. No bands indicating the presence of bound carotenoids were detected in the spectra of Hy8 and XR-L1. Although the spectrum of Hy9 displayed absorption maxima corresponding to carotenoids, their intensity was significantly lower than those of XR. Importantly, the restoration of the DE loop sequence from XR in the Hy81 variant resulted in carotenoid binding similar to that of the recombinant XR (Fig. 8). These findings may indicate changes in the carotenoid binding site in the studied hybrid proteins compared to the carotenoid-bound forms of XR or GR.

Residues located in the extracellular regions of helices E and F, specifically Leu148 from the DE loop, Gly156, Thr160, and Phe163 from helix E, are critical for binding the keto ring and the polyene chain of SX in the XR molecule [8]. There is no homologous residue corresponding to Leu148 in the DE loop sequence of GR [9], which binds native echinenone and other carotenoids. This absence may lead to changes in the configuration of the binding site. In addition, a more compact arrangement of alpha helices in this part of the GR molecule compared to XR may also play an important role. Modeling of the GR-SX complex has revealed that the distance between the ring groups of the carotenoid and retinal is greater in GR than in XR [15]. However, further studies are required to explain the observed effects.

In conclusion, this study demonstrates that optimization of the amino acid sequence of xanthorhodopsin from *S. ruber* based on its homology with stable *Gloeobacter* rhodopsin is an effective strategy to increase the stability of XR variants. We have constructed several hybrid XR variants that exhibit increased stability and improved efficiency of proton transport. Furthermore, we have identified specific regions of the protein sequence that can be modified to specifically alter its functional properties (i.e., photocycle rate and carotenoid binding). Further investigation will help to elucidate the observed effects and provide recommendations for sequence optimization of XR and homologous retinal proteins, aimed at improving their stability in purified form. The hybrid proteins exhibited different photocycle properties, such as the lifetime of the M intermediate, which could be beneficial in applications such as optogenetics.

CRediT authorship contribution statement

Lada E. Petrovskaya: Writing – original draft, Supervision, Resources, Project administration, Investigation, Conceptualization. **Vadim A. Bolshakov:** Writing – original draft, Visualization, Software, Methodology, Investigation. **Evgeniy P. Lukashev:** Writing – original draft, Visualization, Resources, Methodology, Investigation. **Elena A. Kryukova:** Methodology, Investigation. **Eugene G. Maksimov:** Writing – original draft, Supervision, Resources, Project administration, Methodology, Investigation. **Andrei B. Rubin:** Supervision, Resources, Project administration. **Dmitriy A. Dolgikh:** Validation, Supervision, Resources, Project administration. **Sergei P. Balashov:** Writing – original draft, Supervision, Resources, Project administration, Conceptualization. **Mikhail P. Kirpichnikov:** Validation, Supervision, Resources, Project administration, Conceptualization.

Funding

The study was financially supported by the Ministry of Science and Higher Education of the Russian Federation (project no. 075-15-2021-1354) (protein production and spectroscopic studies) and by Russian Scientific Foundation Grant No. 22-14-00104 (mutant genes construction).

Declaration of competing interest

The authors declare no conflict of interest.

Appendix A. Supplementary data

Supplementary data to this article can be found online at https://doi.org/10.1016/j.bbabio.2025.149547.

Data availability

The data are available from the corresponding authors on reasonable request.

References

[1] E.G. Govorunova, O.A. Sineshchekov, H. Li, J.L. Spudich, Microbial rhodopsins: Diversity, mechanisms, and optogenetic applications, Annu. Rev. Biochem. 86 (2017) 845–872.
[2] V. Gordeliy, K. Kovalev, E. Bamberg, F. Rodriguez-Valera, E. Zinovev, D. Zabelskii, A. Alekseev, R. Rosselli, I. Gushchin, I. Okhrimenko, Microbial Rhodopsins, in: V. Gordeliy (Ed.), Rhodopsin: Methods and Protocols, Springer, US, New York, NY, 2022, pp. 1–52.
[3] H. Kandori, Biophysics of rhodopsins and optogenetics, Biophys. Rev. 12 (2020) 355–361.
[4] L.S. Brown, Light-driven proton transfers and proton transport by microbial rhodopsins – A biophysical perspective, Biochim. Biophys. Acta (BBA) - Biomembranes, 1864 (2022) 183867.
[5] S.P. Balashov, E.S. Imasheva, V.A. Boichenko, J. Antón, J.M. Wang, J.K. Lanyi, Xanthorhodopsin: a proton pump with a light-harvesting carotenoid antenna, Science 309 (2005) 2061–2064.
[6] J.K. Lanyi, S.P. Balashov, Xanthorhodopsin: a bacteriorhodopsin-like proton pump with a carotenoid antenna, Biochimica et biophysica acta 1777 (2008) 684–688.
[7] B.F. Lutnaes, A. Oren, S. Liaaen-Jensen, New C40-Carotenoid Acyl Glycoside as Principal Carotenoid in *Salinibacter ruber*, an Extremely Halophilic Eubacterium, J. Nat. Prod. 65 (2002) 1340–1343.
[8] H. Luecke, B. Schobert, J. Stagno, E.S. Imasheva, J.M. Wang, S.P. Balashov, J. K. Lanyi, Crystallographic structure of xanthorhodopsin, the light-driven proton pump with a dual chromophore, Proc. Natl. Acad. Sci. USA 105 (2008) 16561–16565.

[9] E.S. Imasheva, S.P. Balashov, A.R. Choi, K.H. Jung, J.K. Lanyi, Reconstitution of *Gloeobacter violaceus* rhodopsin with a light-harvesting carotenoid antenna, Biochemistry 48 (2009) 10948–10955.

[10] T. Polivka, S.P. Balashov, P. Chabera, E.S. Imasheva, A. Yartsev, V. Sundstrom, J. K. Lanyi, Femtosecond carotenoid to retinal energy transfer in xanthorhodopsin, Biophys. J. 96 (2009) 2268–2277.

[11] S.P. Balashov, E.S. Imasheva, J.M. Wang, J.K. Lanyi, Excitation energy-transfer and the relative orientation of retinal and carotenoid in xanthorhodopsin, Biophys. J. 95 (2008) 2402–2414.

[12] E.S.S. Iyer, I. Gdor, T. Eliash, M. Sheves, S. Ruhman, Efficient Femtosecond Energy Transfer from Carotenoid to Retinal in *Gloeobacter* Rhodopsin–Salinixanthin Complex, J. Phys. Chem. B, 119 (2015) 2345–2349.

[13] S.P. Balashov, E.S. Imasheva, A.R. Choi, K.H. Jung, S. Liaaen-Jensen, J.K. Lanyi, Reconstitution of *Gloeobacter* rhodopsin with echinenone: role of the 4-keto group, Biochemistry 49 (2010) 9792–9799.

[14] K. Chuon, J.-g. Shim, S.-H. Kim, S.-G. Cho, S. Meas, K.-W. Kang, J.-H. Kim, I. Das, M. Sheves, K.-H. Jung, The role of carotenoids in proton-pumping rhodopsin as a primitive solar energy conversion system, J. Photochem. Photobiol. B: Biol., 221 (2021) 112241.

[15] T. Morizumi, W.-L. Ou, N. Van Eps, K. Inoue, H. Kandori, L.S. Brown, O.P. Ernst, X-ray crystallographic structure and oligomerization of *Gloeobacter* rhodopsin, Sci. Rep. 9 (2019) 1–14.

[16] K. Chuon, J.-g. Shim, K.-W. Kang, S.-G. Cho, C. Hour, S. Meas, J.-H. Kim, *A. Choi*, K.-H. Jung, Carotenoid binding in Gloeobacteria rhodopsin provides insights into divergent evolution of xanthorhodopsin types, Commun. Biol., 5 (2022) 1–8.

[17] A. Chazan, I. Das, T. Fujiwara, S. Murakoshi, A. Rozenberg, A. Molina-Marquez, F. K. Sano, T. Tanaka, P. Gomez-Villegas, S. Larom, A. Pushkarev, P. Malakar, M. Hasegawa, Y. Tsukamoto, T. Ishizuka, M. Konno, T. Nagata, Y. Mizuno, K. Katayama, R. Abe-Yoshizumi, S. Ruhman, K. Inoue, H. Kandori, R. Leon, W. Shihoya, S. Yoshizawa, M. Sheves, O. Nureki, O. Beja, Phototrophy by antenna-containing rhodopsin pumps in aquatic environments, Nature 615 (2023) 535–540.

[18] V.A. Boichenko, J.M. Wang, J. Antón, J.K. Lanyi, S.P. Balashov, Functions of carotenoids in xanthorhodopsin and archaerhodopsin, from action spectra of photoinhibition of cell respiration, Biochim. Biophys. Acta (BBA)-Bioenergetics 1757 (2006) 1649–1656.

[19] J.K. Lanyi, S.P., Balashov, Xanthorhodopsin, Halophiles and Hypersaline Environments, Springer, in, 2011, pp. 319–340.

[20] L.E. Petrovskaya, E.P. Lukashev, E.N. Lyukmanova, M.A. Shulepko, E.A. Kryukova, R.H. Ziganshin, D.A. Dolgikh, E.G. Maksimov, A.B. Rubin, M.P. Kirpichnikov, J. K. Lanyi, S.P. Balashov, Expression of Xanthorhodopsin in *Escherichia coli*, Protein J 42 (2023) 408–420.

[21] C. Hour, K. Chuon, M.-c. Song, J.-g. Shim, S.-G. Cho, K.-W. Kang, J.-H. Kim, K.-H. Jung, Unveiling the critical role of K+ for xanthorhodopsin expression in *E. coli*, J. Photochem. Photobiol. B: Biology, 258 (2024) 112976.

[22] T. Tsukamoto, K. Mizutani, T. Hasegawa, M. Takahashi, N. Honda, N. Hashimoto, K. Shimono, K. Yamashita, M. Yamamoto, S. Miyauchi, S. Takagi, S. Hayashi, T. Murata, Y. Sudo, X-ray crystallographic structure of thermophilic rhodopsin: implications for high thermal stability and optogenetic function, J. Biol. Chem. 291 (2016) 12223–12232.

[23] M. Moldenhauer, N.N. Sluchanko, D. Buhrke, D.V. Zlenko, N.N. Tavraz, F. J. Schmitt, P. Hildebrandt, E.G. Maksimov, T. Friedrich, Assembly of photoactive orange carotenoid protein from its domains unravels a carotenoid shuttle mechanism, Photosynth Res 133 (2017) 327–341.

[24] S.A. Siletsky, M.D. Mamedov, E.P. Lukashev, S.P. Balashov, D.A. Dolgikh, A.B. Rubin, M.P. Kirpichnikov, L.E. Petrovskaya, Electrogenic steps of light-driven proton transport in ESR, a retinal protein from *Exiguobacterium sibiricum*, Biochim. Biophys. Acta (BBA)-Bioenergetics, 1857 (2016) 1741–1750.

[25] L.E. Petrovskaya, E.P. Lukashev, V.V. Chupin, S.V. Sychev, E.N. Lyukmanova, E. A. Kryukova, R.H. Ziganshin, E.V. Spirina, E.M. Rivkina, R.A. Khatypov, L. G. Erokhina, D.A. Gilichinsky, V.A. Shuvalov, M.P. Kirpichnikov, Predicted bacteriorhodopsin from *Exiguobacterium sibiricum* is a functional proton pump, FEBS Lett. 584 (2010) 4193–4196.

[26] S.A. Siletsky, E.P. Lukashev, M.D. Mamedov, V.B. Borisov, S.P. Balashov, D.A. Dolgikh, A.B. Rubin, M.P. Kirpichnikov, L.E. Petrovskaya, His57 controls the efficiency of ESR, a light-driven proton pump from *Exiguobacterium sibiricum* at low and high pH, Biochim. Biophys. Acta (BBA)-Bioenergetics, 1862 (2021) 148328.

[27] E.L.G. Samuel, S.L. Holmes, D.W. Young, Processing binding data using an open-source workflow, J. Cheminform. 13 (2021) 99.

[28] D. Bratanov, T. Balandin, E. Round, V. Shevchenko, I. Gushchin, V. Polovinkin, V. Borshchevskiy, V. Gordeliy, An approach to heterologous expression of membrane proteins. the case of bacteriorhodopsin, PloS one 10 (2015) e0128390.

[29] H.E. Kato, F. Zhang, O. Yizhar, C. Ramakrishnan, T. Nishizawa, K. Hirata, J. Ito, Y. Aita, T. Tsukazaki, S. Hayashi, P. Hegemann, A.D. Maturana, R. Ishitani, K. Deisseroth, O. Nureki, Crystal structure of the channelrhodopsin light-gated cation channel, Nature 482 (2012) 369–374.

[30] S. Han, S.-H. Kim, J.-C. Cho, J. Song, G. Bleckner, K.-H. Jung, Photochemical characterization of flavobacterial rhodopsin: The importance of the helix E region for heat stability, Biochim. Biophys. Acta (BBA) - Bioenergetics, 1861 (2020) 148092.

[31] M.R.M. Miranda, A.R. Choi, L. Shi, A.G. Bezerra, K.-H. Jung, L.S. Brown, The Photocycle and Proton Translocation Pathway in a Cyanobacterial Ion-Pumping Rhodopsin, Biophys. J. 96 (2009) 1471–1481.

[32] E.S. Imasheva, S.P. Balashov, J.M. Wang, J.K. Lanyi, Removal and reconstitution of the carotenoid antenna of xanthorhodopsin, J. Membr. Biol. 239 (2011) 95–104.

[33] A.K. Dioumaev, L.S. Brown, J. Shih, E.N. Spudich, J.L. Spudich, J.K. Lanyi, Proton transfers in the photochemical reaction cycle of proteorhodopsin, Biochemistry 41 (2002) 5348–5358.

[34] A.K. Dioumaev, L.E. Petrovskaya, J.M. Wang, S.P. Balashov, D.A. Dolgikh, M. P. Kirpichnikov, J.K. Lanyi, Photocycle of *Exiguobacterium sibiricum* rhodopsin characterized by low-temperature trapping in the IR and time-resolved studies in the visible, The journal of physical chemistry B 117 (2013) 7235–7253.

[35] R. Misra, A. Hirshfeld, M. Sheves, Molecular mechanism for thermal denaturation of thermophilic rhodopsin, Chem. Sci. 10 (2019) 7365–7374.

[36] E.G. Maksimov, M. Moldenhauer, E.A. Shirshin, E.A. Parshina, N.N. Sluchanko, K. E. Klementiev, G.V. Tsoraev, N.N. Tavraz, M. Willoweit, F.J. Schmitt, J. Breitenbach, G. Sandmann, V.Z. Paschenko, T. Friedrich, A.B. Rubin, A comparative study of three signaling forms of the orange carotenoid protein, Photosynth. Res. 130 (2016) 389–401.

[37] V.A. Anashkin, Y.V. Bertsova, A.M. Mamedov, M.D. Mamedov, A.M. Arutyunyan, A.A. Baykov, A.V. Bogachev, Engineering a carotenoid-binding site in *Dokdonia* sp. PRO95 Na(+)-translocating rhodopsin by a single amino acid substitution, Photosynth. Res. 136 (2018) 161–169.

[38] M. le Maire, P. Champeil, J.V. Møller, Interaction of membrane proteins and lipids with solubilizing detergents, Biochim. Biophys. Acta (BBA) - Biomembranes 1508 (2000) 86–111.

[39] A.M. Seddon, P. Curnow, P.J. Booth, Membrane proteins, lipids and detergents: not just a soap opera, Biochim. Biophys. Acta 1666 (2004) 105–117.

[40] Y. Mukai, N. Kamo, S. Mitaku, Light-induced denaturation of bacteriorhodopsin solubilized by octyl-β-glucoside, Prot. Eng. Des. Sel. 12 (1999) 755–759.

[41] T. Kitajima-Ihara, Y. Furutani, D. Suzuki, K. Ihara, H. Kandori, M. Homma, Y. Sudo, *Salinibacter* Sensory Rhodopsin: Sensory rhodopsin I-like protein from a eubacterium, J. Biol. Chem. 283 (2008) 23533–23541.

[42] E.S. Imasheva, S.P. Balashov, J.M. Wang, J.K. Lanyl, pH-dependent transitions in xanthorhodopsin, Photochem. Photobiol. 82 (2006) 1406–1413.

[43] S. Yasuda, T. Akiyama, S. Nemoto, T. Hayashi, T. Ueta, K. Kojima, T. Tsukamoto, S. Nagatoishi, K. Tsumoto, Y. Sudo, M. Kinoshita, T. Murata, Methodology for further thermostabilization of an intrinsically thermostable membrane protein using amino acid mutations with its original function being retained, J. Chem. Inf. Model. 60 (2020) 1709–1716.

[44] J.-g. Shim, K. Choun, K.-W. Kang, J.-H. Kim, S.-G. Cho, K.-H. Jung, The binding of secondary chromophore for thermally stable rhodopsin makes more stable with temperature, Prot. Sci., 31 (2022) e4386.

[45] A.-N. Bondar, J.C. Smith, S. Fischer, Structural and energetic determinants of primary proton transfer in bacteriorhodopsin, Photochem. Photobiol. Sci. 5 (2006) 547–552.

[46] A. Royant, K. Edman, T. Ursby, E. Pebay-Peyroula, E.M. Landau, R. Neutze, Helix deformation is coupled to vectorial proton transport in the photocycle of bacteriorhodopsin, Nature 406 (2000) 645–648.

[47] L.S. Brown, Y. Yamazaki, A. Maeda, L. Sun, R. Needleman, J.K. Lanyi, The proton transfers in the cytoplasmic domain of bacteriorhodopsin are facilitated by a cluster of interacting residues, J. Mol. Biol. 239 (1994) 401–414.

[48] J.-M. Kim, P.J. Booth, S.J. Allen, H.G. Khorana, Structure and function in bacteriorhodopsin: the role of the interhelical loops in the folding and stability of bacteriorhodopsin, J. Mol. Biol. 308 (2001) 409–422.

[49] S.J. Allen, J.-M. Kim, H.G. Khorana, H. Lu, P.J. Booth, Structure and function in bacteriorhodopsin: the effect of the interhelical loops on the protein folding kinetics, J. Mol. Biol. 308 (2001) 423–435.

[50] J.K. Lanyi, H. Luecke, Bacteriorhodopsin, Curr. Opin. Str. Biol. 11 (2001) 415–419.

[51] M. Mehler, F. Scholz, Sandra J. Ullrich, J. Mao, M. Braun, Lynda J. Brown, Richard C.D. Brown, Sarah A. Fiedler, J. Becker-Baldus, J. Wachtveitl, C. Glaubitz, The EF loop in green proteorhodopsin affects conformation and photocycle dynamics, Biophys. J. 105 (2013) 385–397.

[52] J. Stehle, F. Scholz, F. Löhr, S. Reckel, C. Roos, M. Blum, M. Braun, C. Glaubitz, V. Dötsch, J. Wachtveitl, H. Schwalbe, Characterization of the ground state dynamics of proteorhodopsin by NMR and optical spectroscopies, J. Biomol. NMR 54 (2012) 401–413.

[53] H.-J. Steinhoff, R. Mollaaghababa, C. Altenbach, K. Hideg, M. Krebs, H.G. Khorana, W.L. Hubbell, Time-resolved detection of structural changes during the photocycle of spin-labeled bacteriorhodopsin, Science 266 (1994) 105–107.